Correspondence to:
S. Majumder,
sudip.majumder@noaa.gov

Near-inertial kinetic energy budget of the mixed layer and shear evolution in the transition layer in the Arabian Sea during the monsoons

Sudip Majumder[1,2], Amit Tandon[3], Daniel L. Rudnick[4], and J. Thomas Farrar[5]

[1]Cooperative Institute for Marine and Atmospheric Studies, University of Miami, Miami, Florida, USA, [2]Atlantic Oceanographic and Meteorological Laboratory, NOAA, Miami, Florida, USA, [3]Department of Mechanical Engineering, University of Massachusetts Dartmouth, North Dartmouth, Massachusetts, USA, [4]Scripps Institution of Oceanography, University of California, San Diego, California, USA, [5]Woods Hole Oceanographic Institution, Woods Hole, Massachusetts, USA

Abstract We present the horizontal kinetic energy (KE) balance of near-inertial currents in the mixed layer and explain shear evolution in the transition layer using observations from a mooring at 15.26° N in the Arabian Sea during the southwest monsoon. The highly sheared and stratified transition layer at the mixed-layer base varies between 5 m and 35 m and correlates negatively with the wind stress. Results from the mixed layer near-inertial KE (NIKE) balance suggest that wind energy at times can energize the transition layer and at other times is fully utilized within the mixed layer. A simple two layer model is utilized to study the shear evolution in the transition layer and shown to match well with observations. The shear production in this model arises from alignment of wind stress and shear. Although the winds are unidirectional during the monsoon, the shear in the transition layer is predominantly near-inertial. The near-inertial shear bursts in the observations show the same phasing and magnitude at near-inertial frequencies as the wind-shear alignment term.

1. Introduction

Internal waves with frequencies close to the local inertial frequency, or near-inertial waves (NIW), constitute the most energetic part of the internal wave spectrum and are important for transferring energy and momentum from the upper ocean into the interior. Previous studies by *Alford* [2003] and *Watanabe and Hibiya* [2002] suggest that globally, surface winds inject about 0.3–1.4 TW energy into the NIW in the mixed layer, a fraction of which propagates to the interior and helps maintain the abyssal stratification.

Several studies [*Pollard and Millard*, 1970; *D'Asaro*, 1985; *Plueddemann and Farrar*, 2006; *Silverthorne and Toole*, 2008; *Alford et al.*, 2012] present a detailed analysis on the generation, evolution and the propagation of NIW from the upper ocean into the interior. Most of these studies quantify the energy input at the surface using a slab-like mixed layer and are limited to the physical processes occurring only in the mixed layer.

Wind-generated NIW in the upper ocean spans the weakly stratified 'mixed layer' and occasionally penetrate the transition layer, a highly sheared and stratified region between the mixed layer and the upper seasonal thermocline. In a classical slab-like scenario near-inertial currents are uniform with depth in the mixed layer but highly sheared within the transition layer. Such currents in the mixed layer decay with time due to the local dissipation and propagation of NIW from the mixed layer. To understand the input of near-inertial energy fluxes from the wind to the ocean, *D'Asaro* [1985] introduced a one-dimensional model of the mixed layer following *Pollard and Millard* [1970]. *D'Asaro* [1985] showed the forcing of inertial motions is highly intermittent in the mixed layer due to the sensitivity of the inertial response to variations in wind speed and direction. *Plueddemann and Farrar* [2006] (PF06, hereafter) used a similar one-dimensional model of the mixed layer and showed the one-dimensional mixed layer models must incorporate the interaction between the mixed layer and the interior ocean to reproduce the observed NIKE balance. They found that dissipation due to turbulence is the major energy sink in the mixed layer and observed the downward propagation of NIW and remotely generated NIW propagation, at times, can contribute to the mixed layer near-inertial energy budget.

The highly sheared and stratified transition layer often displays $O(1)$ Richardson [*Johnston and Rudnick*, 2008] number leading to instabilities due to enhanced shear. Using a simplified two-layer model. *Burchard and Rippeth* [2009] showed that the alignment of wind and shear can lead to sharp increases in shear variance in a shallow stratified tidal sea. *Brannigan et al.* [2013] expanded this idea in an open ocean context and showed that the simplified two layer construction works well when the upper ocean displays a two-layer structure and the transition layer is highly stratified.

To understand the energy distribution of NIW in the mixed layer and to study the evolution of transition layer thickness (TLT, hereafter) and shear in it, we analyze data from a mooring array near 15.7°N in the Arabian Sea and use results from a one dimensional model of the mixed layer forced with the observed fluxes and initialized with temperature and salinity profiles. The Arabian Sea experiment was conducted for a year between October 1994 and October 1995 including both the wintertime northeast and the summertime southwest monsoon to understand the air-sea interaction in this region, and in particular to understand the oceanic response to the large-scale atmospheric forcing associated with monsoon. The data used in this study span both the transition period with low winds and the period of extremely strong winds at the peak of the southwest monsoon. It also enables us to study the generation and evolution of near-inertial currents in the mixed layer and shear in the transition layer in a tropical unidirectional wind forcing regime which is different from the midlatitude studies of isolated storms with rotating winds.

The paper is structured as follows. We discuss the data used in this study in section 2. In section 3, we present the TLT time series based on maximum shear and stratification and explain their evolution during the southwest monsoon. We derive the energy balance of near-inertial currents in the mixed layer in section 4 and explain the near-inertial energy evolution in the transition layer in section 5. Sections 6 and 7 discuss the production and destruction of shear in the transition layer. We summarize and discuss our results in section 8.

2. Data

To understand the air-sea interaction and oceanic response to the large scale atmospheric forcing, an array of five moorings in the Arabian Sea was deployed. The mooring array yielded yearlong time series of atmospheric and oceanic variables spanning the wintertime northwest and summertime southwest monsoon in the Arabian Sea from October 1994 to October 1995. The five moorings in the array were deployed in a square of 55 km sides, centered at (15.5°N, 61.5°E). The Upper Ocean Processes Group, Woods Hole Oceanographic Institution (WHOI) deployed the heavily instrumented central mooring and the other four moorings, two in the east and two in the west, were deployed by University of Washington and Scripps Institution of Oceanography (SIO). In this study we mainly use observations from the SIO south mooring (SIO-S) at 15.26° N, 61.26° E. This mooring provides time series of sea surface temperature (SST) every 7.5 min, subsurface temperature every 15 min at 10, 20, 30, 40, 50, 70, 90, 110, 130, 150, 170, and 190 meters, and currents. A downward facing ADCP at 1.5 m covered a depth between 8 m and 124 m and recorded currents every 4 m. The processed ADCP currents have 15 min temporal resolution. We obtain the wind stress data from meteorological measurements using a COARE-Met Flux algorithm [*Fairall et al.*, 1996] every 7.5 min.

Since salinity data are not available at SIO-S and mixed-layer depth at SIO-S and at the central WHOI mooring are about the same, we use salinity data from the central mooring (courtesy, Robert Weller/WHOI) measured at depths: 1.8, 10, 35, 65, 80, 100, 150, 200 and 250 meters at 15 min intervals.

3. Shear and Stratification-Based Transition Layer Thickness

TLT is defined in literature in several ways, for an example, *Johnston and Rudnick* [2008] define TLT based on mixed-layer depth (MLD, hereafter) variations, momentum transport depth, strength of shear and stratification at the mixed-layer base using Sea-Soar data. *Dohan and Davis* [2011] use a temperature criteria to define the transition layer.

Following *Johnston and Rudnick* [2008], we estimate TLT based on maximum shear and stratification at the mixed-layer base as, $TLT_{S^2_{max}} = z(S^2_{max}) - z(MLD)$, and $TLT_{N^2_{max}} = z(N^2_{max}) - z(MLD)$. Where $S = \sqrt{\left(\frac{\partial u}{\partial z}\right)^2 + \left(\frac{\partial v}{\partial z}\right)^2}$ is shear, and u and v are eastward and northward velocities and z is depth. Density stratification strength (N^2)
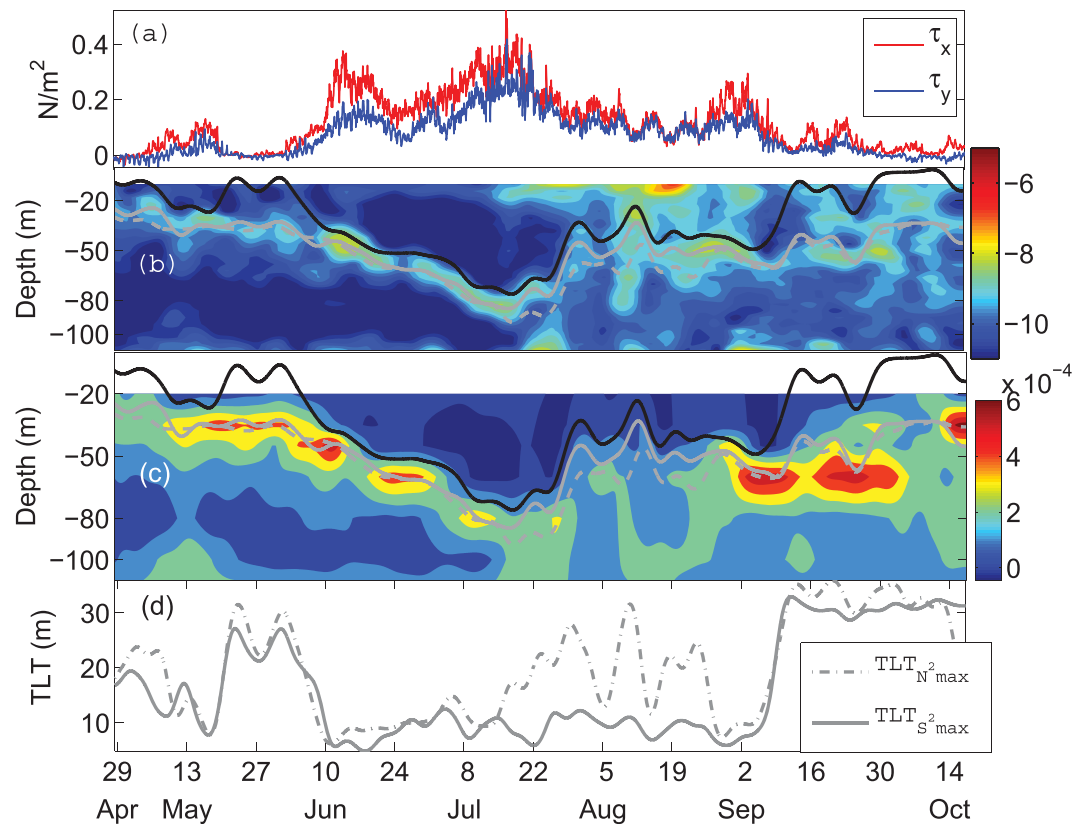
Figure 1. (a) Hourly wind-stress components (τ_x, τ_y) at the mooring location. (b) Weekly averaged shear-squared (color) in logarithmic scale overplotted with weekly MLD (black solid line), maximum shear (gray solid line), and maximum stratification (gray dash-dots line) depths. (c) Weekly averaged stratification-squared (color) overplotted with weekly MLD (black), maximum shear (gray), and stratification (gray dash-dots) depths. (d) Weekly $TLT_{S^2_{max}}$ (solid gray line) and $TLT_{N^2_{max}}$ (gray dash-dots line).

is related to the vertical gradient of density $\frac{\partial \rho}{\partial z}$ as, $N^2 = -\frac{g}{\rho_o}\frac{\partial \rho}{\partial z} = g\beta\frac{\partial s}{\partial z} - g\alpha\left(\frac{\partial T}{\partial z} + \Gamma\right)$, where $\alpha = -\frac{1}{\rho_0}\frac{\partial \rho}{\partial T}$ and $\beta = \frac{1}{\rho_0}\frac{\partial \rho}{\partial s}$, in which g, s, T, ρ, and Γ [Gill, 1982] are gravity, salinity, temperature, depth, density and adiabatic temperature gradient respectively, and ρ_0 is the reference density.

We estimate MLD as the depth where the temperature changes by 0.1°C from the surface. The estimated MLD has a mean value of 32 m and varies from 1.01 to 91 m with a standard deviation of 22 m. The transition layer thickness varies between 5 m during the strongest winds at the peak of the southwest monsoon and 35 m in the pre-monsoon period. The TLT values observed in this study are similar to that (8–24 m) observed by *Johnston and Rudnick* [2008]. Since the vertical resolution of shear and stratification are 4 m and about 10–15 m respectively, the TLT estimates involve errors due to interpolation. $TLT_{S^2_{max}}$ is relatively well resolved, therefore all the calculations shown in the following sections involving TLT are based on $TLT_{S^2_{max}}$.

3.1. Evolution of TLT During the Transition Period and in the Southwest Monsoon
The transition period in April and May is characterized by weak winds. Weak winds and strong surface heating (not shown) [*Fischer et al.*, 2002] during this period create a shallow mixed layer. As the winds strengthen during the summertime southwest monsoon (in June, July, and August) mixed layer deepens. The net heat flux during the transition period and in the southwest monsoon varies between -25 W/m^2 and 200 W/m^2 (not shown). *Fischer* [1997] shows that the net heat flux during the transition period balances the integrated heat content of the water-column, but this balance deviates during the southwest monsoon in June and July.

The wind stress varies from 0.0 to 0.6 N/m^2 from the transition period to the peak of the southwest monsoon (Figure 1a). The MLD is strongly correlated with the wind stress (correlation coefficient = 0.9). Shear
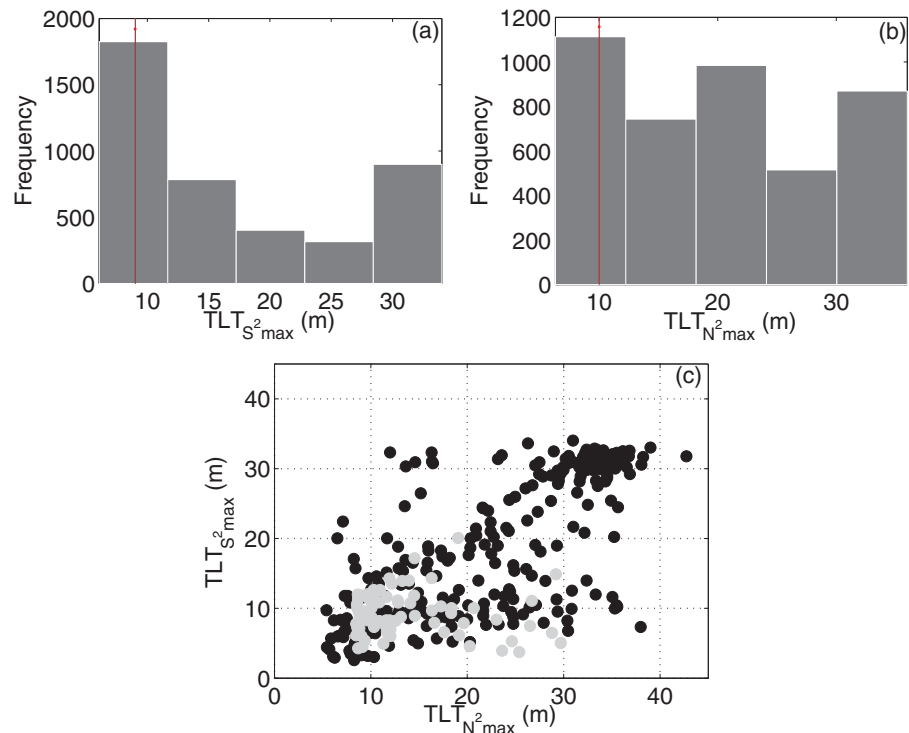
Figure 2. (a, b) Histograms of weekly averaged $TLT_{S^2_{max}}$ and $TLT_{N^2_{max}}$. The modes (about 10 m) are shown by thin red vertical lines. (c) Scatter plot of 12 h block-averaged $TLT_{S^2_{max}}$ and $TLT_{N^2_{max}}$. Black and gray circles represent TLT values when MLD varies between 0 and 50 m and greater than 50 m respectively. TLTs are well correlated for shallower MLD but the correlation is weak for deeper MLD.

within the mixed layer is weak, but a strong, persistent shear layer, correlated strongly with the wind-stress magnitude, is observed at the mixed-layer base (Figure 1b). This persistent shear layer is highly stratified (Figure 1c). When wind stress is weak and mixed layer is shallow, TLT is thick. During the strong forcing events mixed layer deepens and a thin transition layer is sustained below.

$TLT_{N^2_{max}}$ and $TLT_{S^2_{max}}$ are well correlated (correlation coefficient = 0.8) and yield a 10 m mode TLT (Figures 1d and 2). The correlation is even stronger (correlation coefficient = 0.87) when wind is weak and mixed layer is shallow. However, the correlation is weak when MLD is deep. Figure 2 shows $TLT_{S^2_{max}}$ is roughly constant for MLD > 50m. This perhaps suggests that wind energy only penetrates so deep, and once the mixed layer is deep enough TLT evolution may be decoupled from the wind forcing. Both measures of TLT exhibit negative correlation with the wind-stress magnitude (Figure 1d). This is because TLT decreases as strong wind deepens the mixed layer and erodes the shear layer at its base (Figure 1). Strong shear and stratification in the transition layer often suggest $O(1)$ Richardson numbers (defined as $Ri = N^2/S^2$) that indicate shear based instability can occur in the transition layer (Figure 3).

4. Near-Inertial Kinetic Energy Budget of the Mixed Layer

In this section, we present the near-inertial kinetic energy budget of the mixed layer and discuss the importance of different energy partition terms in the budget using a bulk approximation of the mixed layer. The momentum equation of a slab-like mixed layer (thickness, H) subjected to wind-forcing (τ_W^x, τ_W^y) and bottom-stress (τ_R^x, τ_R^y) in complex notation is,

$$\frac{dZ}{dt} + if\,Z = \frac{T_W - T_R}{H} \tag{1}$$

where $Z = u + iv$ is the mixed layer current, $T_W = (\tau_W^x + i\tau_W^y)/\rho$ is the complex wind stress, f is the Coriolis frequency. T_R represent the momentum fluxes associated with all the processes in the mixed layer and in the transition layer. These processes in general include dissipation in the mixed layer, vertical propagation of
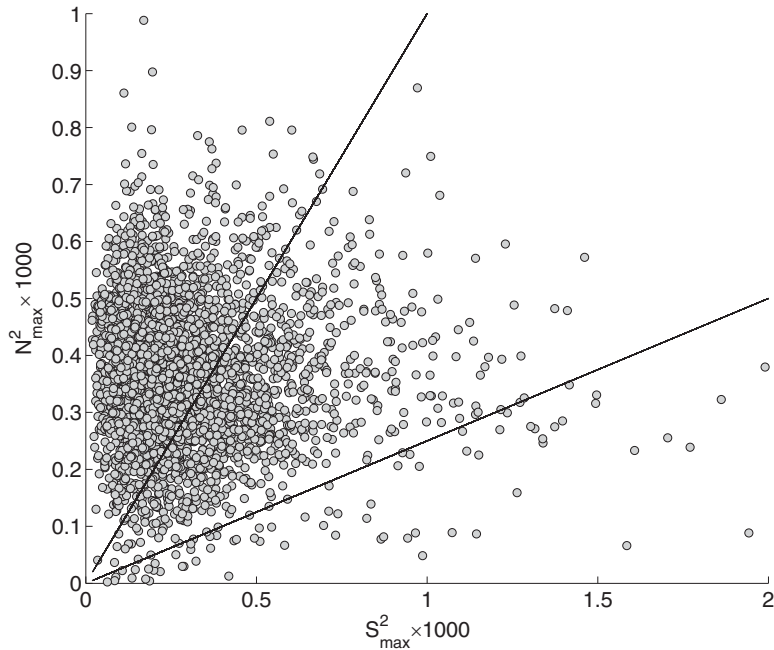
Figure 3. Scatter plot of maximum N^2 and S^2 in the transition layer. Black sloping lines indicate, Ri=1 (high slope) and 0.25 (low slope).

NIW by inertial pumping and momentum transfer between the mixed layer and the transition layer caused by the turbulent stresses (PF06).

To obtain the near-inertial momentum equation we band pass (1) over the near-inertial frequency band [*Silverthorne and Toole*, 2008] and obtain equation (2), the complex near-inertial momentum equation for a slab-like mixed layer.

$$\frac{dZ_I}{dt} + if\, Z_I = \frac{T_{WI} - T_{RI}}{H}. \tag{2}$$

The near-inertial current (Z_I) in the mixed layer is calculated by bandpassing currents 8 m below the surface using a fourth-order Butterworth band pass filter with a passband $0.8f - 1.2f$ (local inertial period = 45 h). This choice of passband is used because the horizontal velocity spectra (not shown) contains most of the near-inertial energy in $0.8f - 1.2f$ frequency range. Near inertial wind stress τ_I is isolated using the same procedure.

Multiplying both sides of (2) by $\rho H Z_I^*$ we obtain an energy equation of the mixed layer (3):

$$\frac{d(NIKE_{ML})}{dt} + if\,\rho H |Z_I|^2 = \rho Z_I^* T_{WI} - \rho Z_I^* T_{RI} + \frac{1}{2}\rho |Z_I|^2 \frac{dH}{dt}. \tag{3}$$

$NIKE_{ML} = \frac{1}{2}\rho H |Z_I|^2$ is the near-inertial kinetic energy of the mixed layer. $NIKE_{ML}$ varies only on low frequencies (with our passband limits, $NIKE_{ML}$ variations occur between 0 and 0.4 f).

Considering the real part of (3),

$$\frac{d(NIKE_{ML})}{dt} = Re\left(\rho Z_I^* T_{WI} - \rho Z_I^* T_{RI}\right) + \frac{1}{2}\rho |Z_I|^2 \frac{dH}{dt},$$

$$\frac{d(NIKE_{ML})}{dt} = \Pi_W + \Pi_R + \Pi_H, \tag{4}$$

where

$$\Pi_W = Re\left(Z_I^* \tau_{WI}\right), \quad \Pi_R = -Re\left(Z_I^* \tau_{RI}\right), \quad \text{and} \quad \Pi_H = \frac{1}{2}\rho |Z_I|^2 \frac{dH}{dt}. \tag{5}$$

Equation (4) represents the horizontal kinetic energy balance of near-inertial currents in the mixed layer. Π_W is the energy flux from the wind transferring energy to the mixed layer near inertial currents. Π_W derived above, is different from the Π_W estimated in previous studies (discussed in the Appendix A).
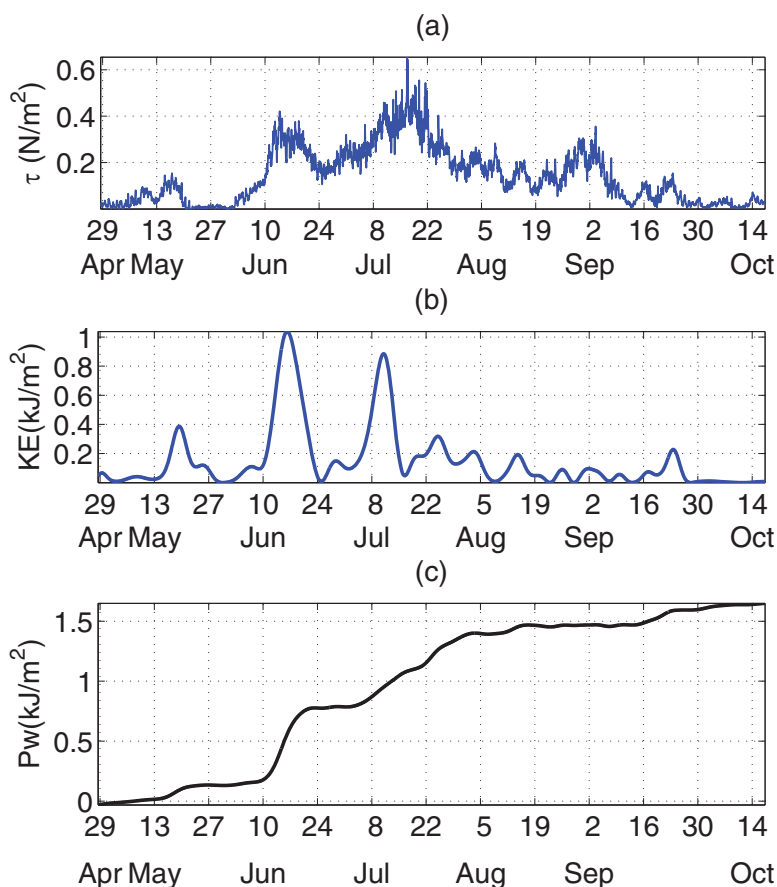
Figure 4. (a) Magnitude of wind stress, (b) Mixed layer NIKE, (c) P_W (Π_W integrated in time).

T_R is unknown and therefore we can not calculate Π_R from (5). We calculate Π_R as a residual flux from (4). Π_R accounts for the change in $NIKE_{ML}$ due to all such processes that add or remove energy from the mixed layer, including advection and radiation losses. H is weekly filtered MLD and Π_H in (5) is the energy flux due to change in MLD (H) with time (PF06). Thus, this study is restricted to slowly varying MLDs.

We estimate all energy partition terms in (4) using both observations and results from a one-dimensional mixed-layer model by *Price et al.* [1986] (PWP). For the model calculations, the salinity and temperature profiles on 29 April are used for initialization and forced with observed wind stress, heat and fresh water fluxes, with a 1 m vertical resolution at hourly intervals until 24 June. To account for the radiation losses associated with downward propagating NIW, we include a linear damping term, -rZ in the model momentum equation, where r is equivalent to 2 inertial periods (4 days). The parameter r is added in the PWP model to mimic the downward propagation of radiation and to prevent inertial oscillations cut off from the forcing and mixed layer from ringing forever. Due to the presence of strong horizontal gradients of temperature [*Fischer et al.*, 2002] at the mooring site after 24 June, there are large differences between the PWP model and the observations and those model results are not reported here.

Following a similar procedure as with the observations we estimate the energy partition terms using PWP model results. To obtain a cumulative estimate of windwork, we integrate Π_W over time. The integrated windwork $P_W (= \int \Pi_W dt)$ has a step-like structure with varying step heights (Figure 4c). Bigger step heights indicate strong forcing events with more energy input into the mixed layer (Figures 4b and 4c). Later in July when the wind stress is at its peak, cumulative windwork is maximum showing a 0.6 kJ increase in step height (Figure 4c).

Figure 5 shows the time series of energy partition terms, contours of the shear of near-inertial velocities and the mean shear in the transition layer. Shear in the mixed layer is extremely weak at near-inertial
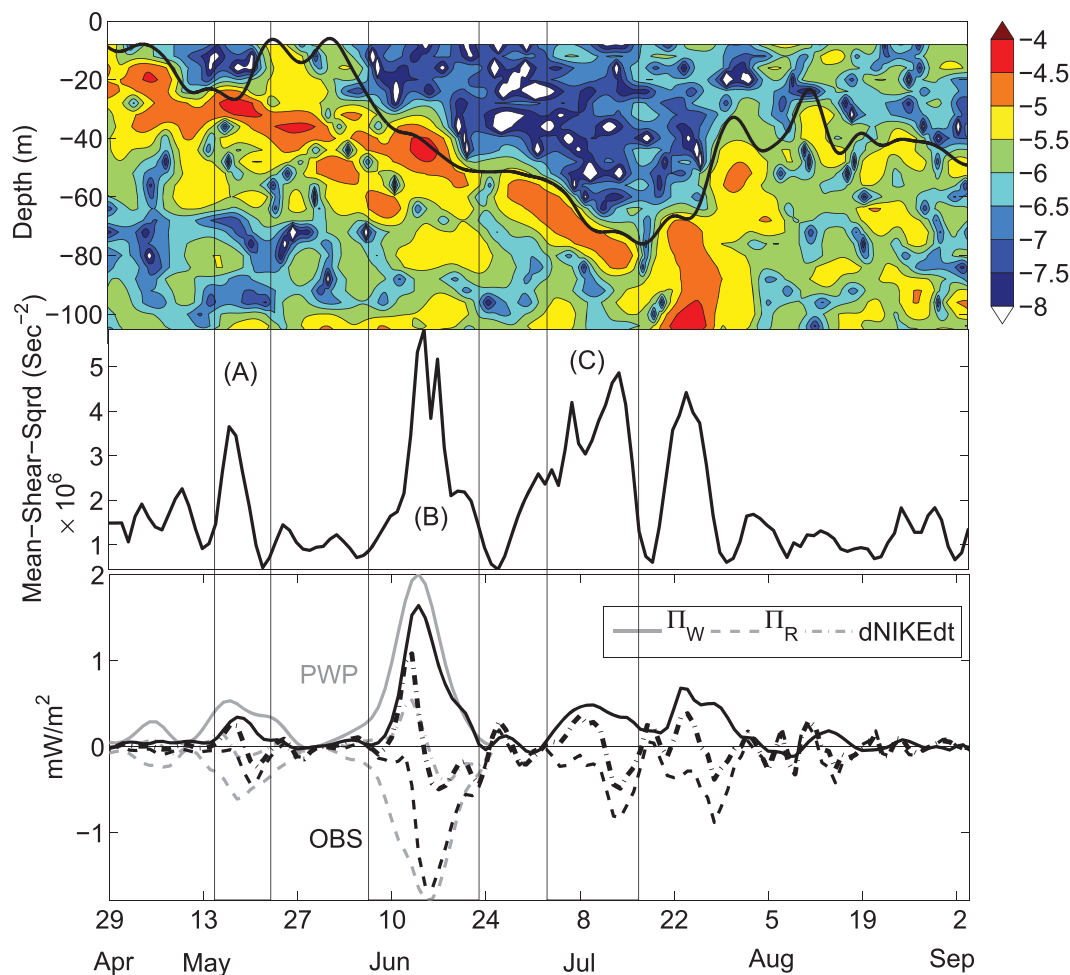
Figure 5. (top) magnitude of near-inertial shear-squared (contours, in logarithmic scale) and MLD (thick black line) with depth. (middle) mean shear-squared in the shear based transition layer. (bottom) observations (black) and PWP model (gray) estimates of Π_W, Π_R and rate of change in NIKE in the mixed layer.

frequencies (Figure 5, top), but exhibits high values in the transition layer. This high shear in the transition layer results from the difference between amplitudes of near-inertial currents in the mixed layer and in the transition layer.

We observe large Π_W and high mean shear in the transition layer at the same time (Figure 5, middle and bottom). The residual flux Π_R is mostly negative indicating energy loss to turbulent dissipation in the mixed layer and the radiation of NIW away from the mixed layer.

Although the energy partition terms from the model and observations show similar fluctuations (Figure 6a), the model overestimates the windwork (Figure 6b) and predicts a weaker NIKE change in the mixed layer $\left(\frac{dNIKE}{dt}_{ML}\right)$ than the observations. The model residual flux Π_R is stronger but at times (14–23 June) exhibits similar values (between 0 and 1.4 mW/m^2) as Π_R from the observations. Since PWP model has no advection, this result suggests that Π_R during this period is determined by dissipation in the mixed layer and downward radiation losses of NIW from it.

It is plausible that the discrepancy between the observations and PWP model arises due to the presence of background near-inertial currents at the mooring site. In general, the background near-inertial currents can diminish or enhance the total windwork based on whether they oppose the wind or are in the same direction. The model windwork Π_W is stronger because the currents are only generated by the wind stress in the model.

To examine the energy flux into or out of the transition layer, we choose to analyze three events, which are marked A to C (Figure 5, middle).
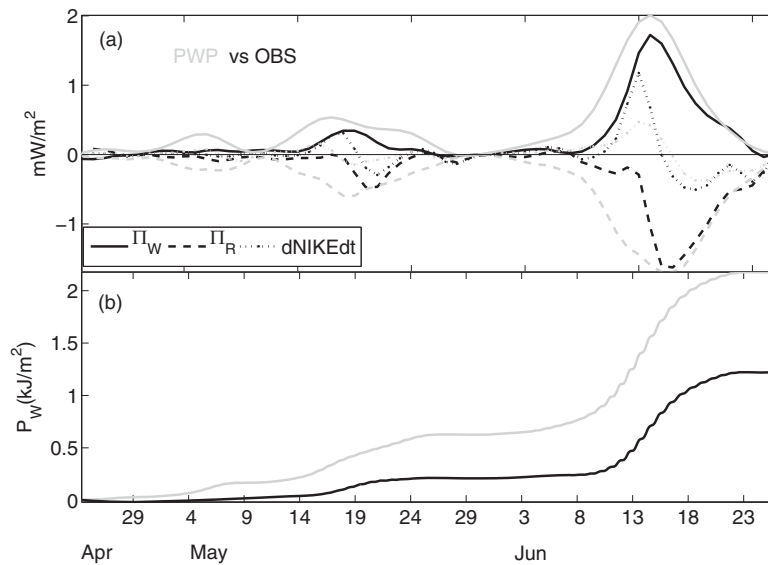
Figure 6. (a) Mixed layer energy budget terms from the model (gray) and the observations (black). Windwork and the residual (Π_R) from the model is higher than the observations. Model Π_R matches the observations from 15 to 25 June, suggesting the processes that determine Π_R in the model could also be important in real ocean during this period. (b) Integrated windwork from model and the observations.

5. Importance of Π_R to the Energy and Shear Evolution in the Transition Layer

In the previous section we described Π_R as a residual representing the energy loss in the mixed layer. In this section we investigate the role of Π_R to the energy evolution in the transition layer for events A, B and C.

5.1. Event A

Event A occurs during the quiet phase of the southwest monsoon, when the wind stress varies between 0.0 N/m^2 and 0.1 N/m^2. The MLD at the beginning of this event is about 30 m, but shoals as the wind weakens from 20 to 25 May. TLT during this event ranges between 10 m and 30 m. Strong winds and enhanced windwork between 14 and 18 May steadily increase the NIKE in the mixed layer (Figure 7). The rate of change in NIKE of the transition layer $\left(\int \frac{\partial (\frac{1}{2}\rho |Z_{TL}|^2)}{\partial t} dz \right)$ is positive and nearly matches -Π_R (Figure 7, bottom) between 14 and 23 May. The small difference (about 0.2mW/m^2) is due to the rapid change in MLD (Π_H=0.2 mW/m^2) during this period.

Wind stress decreases to its minimum value ($\sim$ 0 N/m^2) on 20 May. With decreasing windwork the NIKE change in the mixed layer is negative. The residual flux during this period is strong with a maximum 0.6 mW/m^2 on 20 May when NIKE in the mixed layer does not change. The change in NIKE in the transition layer equals the residual flux on 20–23 May; thereafter the NIKE change becomes negative. This decrease in NIKE in the transition layer can be attributed to the processes that remove energy from the transition layer. As the wind stress decreases after 18 May, mixed layer shoals reaching the surface. A relic mixed layer, estimated as a layer where the temperature changes by 1°C (white dash-dots, Figure 7, middle) from the surface, does not show a similar shoaling as seen in the mixed layer (20–27 May). The region between the mixed and the relic layer thickens on 21–27 May when the change in NIKE in the transition layer is negative. The thickening of the transition layer associated with a decrease in KE suggests a mixing event. However, since we do not have well resolved density data, Richardson number cannot be evaluated.

5.2. Event B

Event B occurs during the onset of the southwest monsoon in the Arabian Sea when wind stress is strong (0.1–0.4 N/m^2) and the input wind energy flux is maximum (1.55 mW/m^2). Strong wind forcing during this event deepens the mixed layer resulting a thin (5–7 m) transition layer below. The windwork at the beginning of this event enhances the KE of the mixed layer (10–13 June). This enhanced KE lasts for about two inertial periods but does not increase the NIKE in the mixed layer further. The rate of NIKE change in the mixed layer is zero on 16 June and negative thereafter. The residual flux Π_R becomes maximum
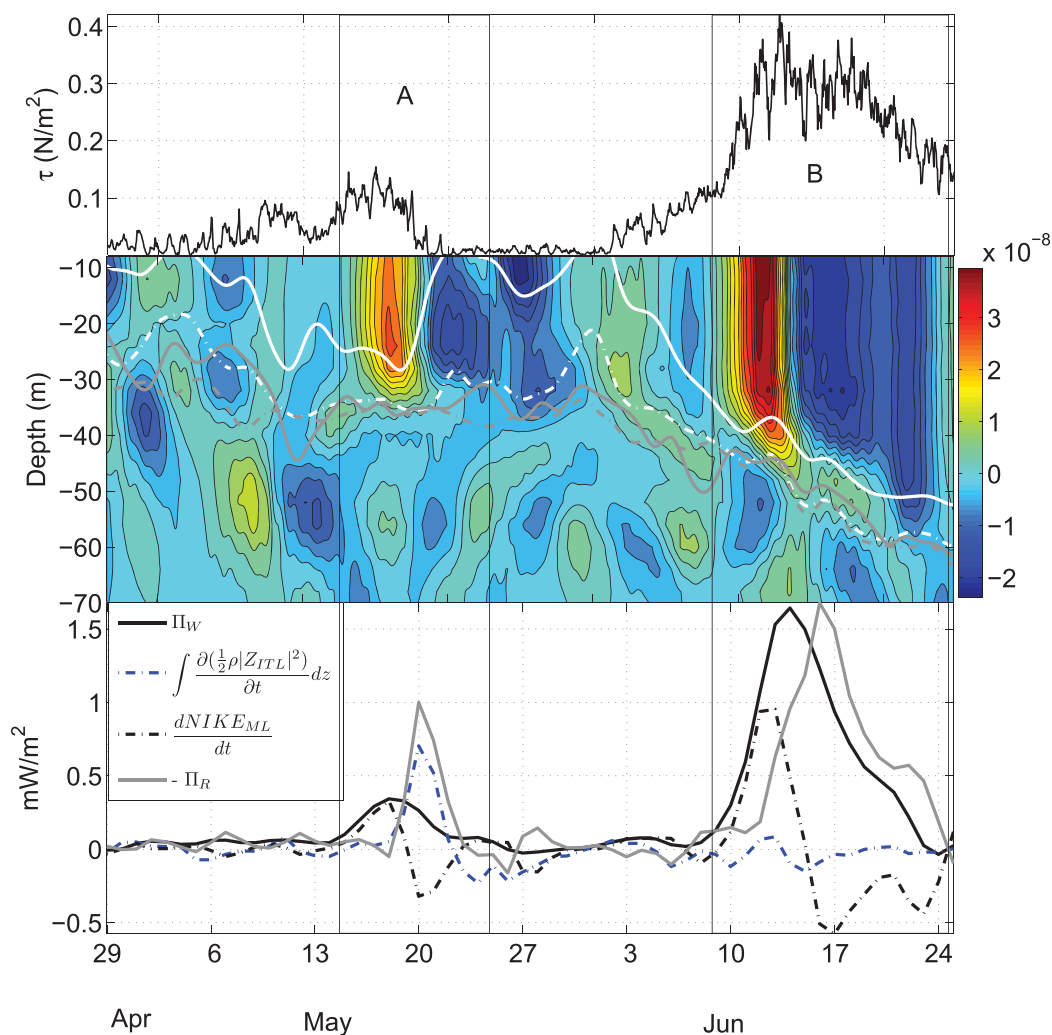
Figure 7. Processes influencing NIKE balance in the mixed layer and in the transition layer during event A and B. (top) magnitude of hourly wind stress. (middle) contours of rate of change in near-inertial kinetic energy (m^2/s^3) overplotted with mixed layer (solid white), the relict mixed layer (white dash-dot line), maximum shear (gray dash-dot line) and maximum stratification depths (solid gray line). (bottom) Π_W, $-\Pi_R$, $\frac{dNIKE_{ML}}{dt}$, and $\int \frac{\partial(\frac{1}{2}\rho|Z_{TL}|^2)}{\partial t} dz$.

(1.5 mW/m^2) on 16 June during this event. Π_R during this event mostly accounts for dissipation in the mixed layer (shown in section 4); the transition layer receives little energy. $\int \frac{\partial(\frac{1}{2}\rho|Z_{TL}|^2)}{\partial t} dz$ therefore is weak at the beginning of this event and becomes zero after 17 June.

5.3. Event C

Event C occurs between 4 July and 16 July when the southwest monsoon in the Arabian Sea was the strongest (Figure 8). Significantly large windwork deepens the mixed layer (about 70 m) and deposits strong near-inertial shear in the transition layer. During event C the residual flux is strong. However, the thin transition layer does not show any change in NIKE. TLT exhibits a strong negative correlation (correlation coefficient =0.7) with the magnitude of the wind stress for the entire time series. This is because during strong wind events the mixed layer deepens and erodes the transition layer at its base; by contrast during the weak wind events the mixed layer shoals and a thicker transition layer develops.

The transition layer is thin (about 5 m) during events B (9–24 June) and C (4–16 July) and shows negligible change in NIKE (Figure 7, bottom). The residual flux however is significantly large due to NIKE losses in the mixed layer.
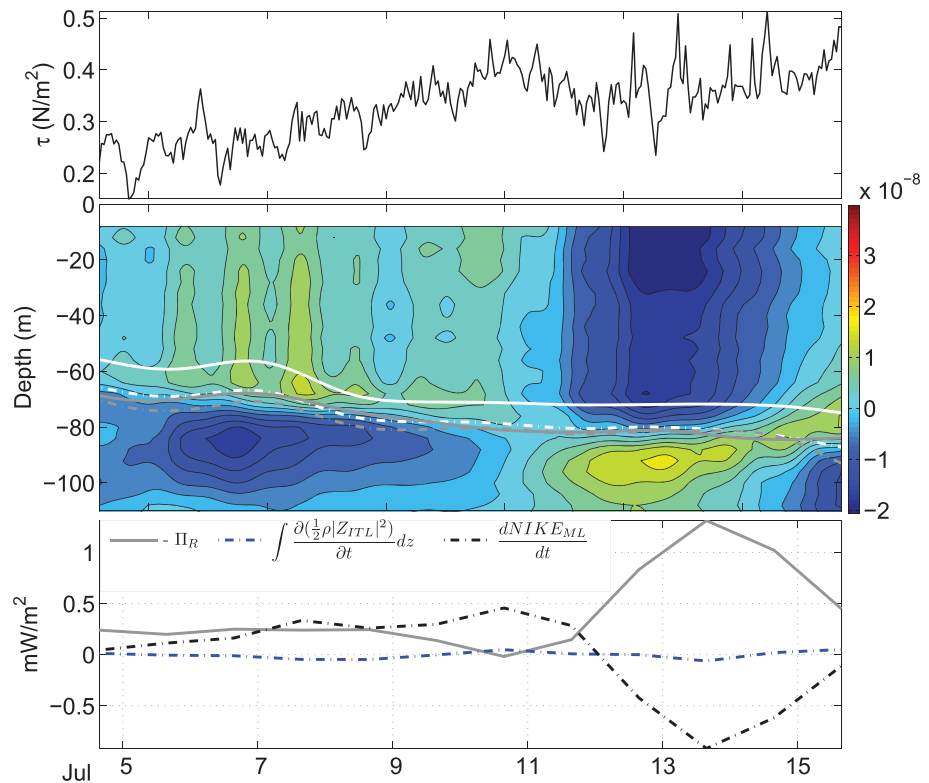
Figure 8. (top) magnitude of hourly wind stress. (middle) Same as the middle plot of Figure 7 for event C. (bottom) $-\Pi_R$, $\frac{dNIKE_{ML}}{dt}$, and $\int \frac{\partial(\frac{1}{2}\rho|Z_{ml}|^2)}{\partial t} dz$.

6. Shear Evolution in the Transition Layer

In this section, we study the evolution of near-inertial shear in the transition layer using a two-layer model following *Brannigan et al.* [2013] and *Burchard and Rippeth* [2009]. In a strictly two layer system the transition layer is infinitesimally thick, but we assume that as layer thickness goes to zero, the shear across this layer becomes infinite, such that the velocity difference across the transition layer is finite. This model describes the shear spikes across the transition layer when the upper ocean shows a two-layer structure. The model assumes that the bulk-mixed-layer moves in response to the wind stress but the layer below is quiescent.

The momentum equations for the two layer model are,

$$\frac{\partial Z_s}{\partial t} + if\ Z_s = \frac{T_W - T_i}{H}, \tag{6}$$

for the upper layer and,

$$\frac{\partial Z_l}{\partial t} + if\ Z_l = \frac{T_i}{h_l}, \tag{7}$$

for the lower layer. Where T_i is the interfacial stress [*Burchard and Rippeth*, 2009; *Brannigan et al.*, 2013], h_l is the thickness of the lower layer and $Z_s(=u_s+iv_s)$ and $Z_l(=u_l+iv_l)$ are depth-averaged complex horizontal currents in the upper and the lower layers. The complex bulk shear between the layers is,

$$S = \frac{Z_s - Z_l}{h}, \tag{8}$$

where h is the distance between the center of mass of the upper layer and lower layer (below the transition layer). Substituting (8) by subtracting (6) and (7) and dividing h both sides, we obtain,

$$\frac{\partial S}{\partial t}+ifS=\frac{T_W}{hH}-\frac{T_i}{Hh_l}.$$ (9)

Multiplying S^* (complex conjugate of S) both sides and only considering the real parts, (9) can be expressed in terms of vector dot products as,

$$\frac{\partial S^2}{\partial t}=2\left(\frac{\mathbf{S.T_W}}{Hh}\right)-2\left(\frac{\mathbf{S.T_i}}{Hh_l}\right).$$ (10)

where $\mathbf{S.T_W}=S^*T_W=S_xT_W^x+S_yT_W^y$ and $\mathbf{S.T_i}=S^*T_i=S_xT_i^x+S_yT_i^y$; S_x and S_y are the zonal and meridional components of the bulk shear. The S^2 evolution (10) can be written in terms of shear production and destruction as,

$$\frac{\partial S^2}{\partial t}=P(S^2)-D(S^2),$$ (11)

where $P(S^2)=2\left(\frac{\mathbf{S.T_i}}{Hh}\right)$ and $D(S^2)=2\left(\frac{\mathbf{S.T_i}}{Hh_l}\right)$ are S^2 production/destruction (depending on the wind and shear direction) and destruction by interfacial friction. Following *Brannigan et al.* [2013], the interfacial friction body force is parameterized as,

$$T_i=c_i(Z_s-Z_l)|Z_s-Z_l|=c_ih^2\mathbf{S}|S|,$$ (12)

where c_i is the drag coefficient. Substituting (12) in (10) we get,

$$\frac{\partial S^2}{\partial t}=2\left(\frac{\mathbf{S.T_W}}{hH}-c_i\frac{h^2}{Hh_l}|S^3|\right).$$ (13)

Near-inertial components are obtained by bandpassing (13) as,

$$\frac{\partial S_l^2}{\partial t}=2\left(\frac{\mathbf{S.T_W}}{hH}\right)_l-2\left(c_i\frac{h^2}{Hh_l}|S^3|\right)_l.$$ (14)

We estimate both $\frac{\partial S^2}{\partial t}$ and $2\left(\frac{\mathbf{S.T_W}}{hH}\right)$ and the near-inertial components of these terms in (14) using observations. We use weekly filtered MLD and TLT and the same near-inertial passband (as used in section 4) to estimate these terms. In Appendix B, we present a scale analysis of the second term in the right of (13) and (14) and show that these terms are 7 orders of magnitude smaller than the others and not important to the shear evolution.

7. Results From Shear Evolution Model

Figure 9 shows the evolution of bulk-shear $(\frac{\partial S^2}{\partial t})$ across the transition layer from 9 May to 25 July. The square of the mean-bulk-shear (S^2, Figure 9, second plot) is intermittent and displays multiple spikes with amplitude ranging from $(0.1–0.6) \times 10^{-4}s^{-2}$. After 4 July the production of S^2 is weak as the shear alignment is not high (Figure 9, fourth plot). The maximum S^2 (0.6×10^{-4} s^{-2}) is observed in event B on 13 June when the wind stress is about 0.4 N/m^2. The shear production term $P(S^2)$ is less than the shear evolution $\left(\frac{\partial S^2}{\partial t}\right)$ in the transition layer, but the phases of the two terms are in good agreement throughout the time series. Unidirectional monsoon winds disallow the resonance between rotation of the wind and earths rotation which is the cause of amplification of near-inertial currents in midlatitudes [*Dohan and Davis*, 2011]. In the Arabian sea, the time variation of wind stress and rotation of the bulk shear across the transition layer (Figure 9, fourth plot) cause the increase in magnitude of the bulk shear across the transition layer when this shear and wind stress are aligned.

The near-inertial components of shear evolution and production are shown in Figure 10. Maximum near-inertial $S_l^2(\sim 0.12\times10^{-4}s^{-2})$ is observed between 13 and 15 June, during event B. Other shear spikes during events A and B can reach upto $1.5\times 10^{-6}s^{-2}$. The results from the model are in better agreement with the observations in the near-inertial frequency band showing similar phase and amplitude for the shear production and evolution. These results show that the high stratification in the transition layer allows a two layer system to be a good approximation, particularly for describing the spikes in the near-inertial shear in terms of alignment of shear and wind stress vectors.
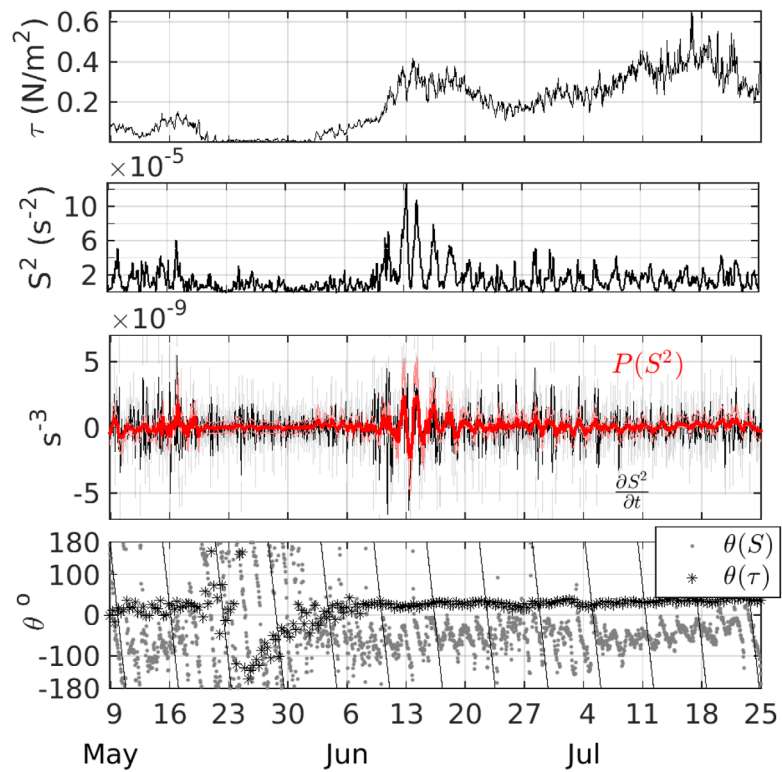
Figure 9. (first) Hourly wind stress; (second) 4 h low-passed S^2; (third) 4 h low-passed shear production $P(S^2)$ (red) and $\frac{\partial S^2}{\partial t}$ (black). Gray and pink shades are uncertainties associated with $P(S^2)$ and $\frac{\partial S^2}{\partial t}$; (fourth) direction of wind (black stars) and bulk shear (gray dots). The black sloping lines indicate local inertial rotation.

8. Summary and Discussions

We estimate the NIKE budget of the mixed layer and explain the shear evolution in the transition layer using data from a mooring in the Arabian Sea during the monsoon season. Extremely strong, unidirectional monsoon winds in the Arabian Sea make this region different than the regions in the mid latitude with storms that last for few days, associated with winds that are not unidirectional.
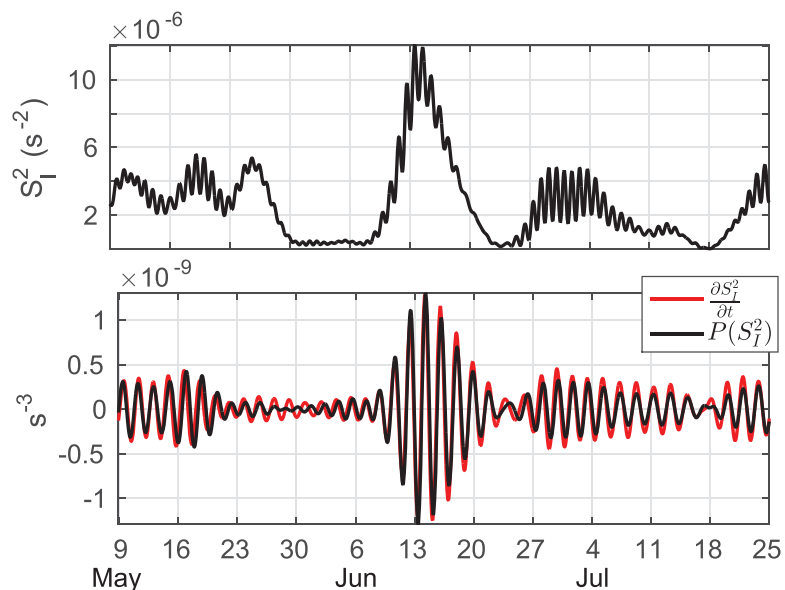

Figure 10. (top) S_I^2, the near-inertial part of S^2; (bottom) shear production $P(S_I^2)$ (black) and $\frac{\partial S_I^2}{\partial t}$ (red) for the near-inertial frequency band.

The wind-forced mixed layer is shallow during the quiet periods of the southwest monsoon but deepens upto 70 m when the wind stress reaches a maximum at the peak of the southwest monsoon. Below the mixed layer there exists a highly sheared and stratified transition layer. The thickness of this layer depends on the variations in the wind-modulated MLD and shows values between 5 m and 35 m. In the transition period (in April–May) the mixed layer is shallow with a 10–35 m thick transition layer below it. As the wind stress increases after the transition period, in the southwest monsoon, the mixed layer deepens and erodes the transition layer below.

Several studies in the midlatitudes [*Alford et al.*, 2012; *Dohan and Davis*, 2011] document the evolution of near inertial currents that are generated mostly by short-duration storms and by rotating winds. Alternatively, *Weller et al.* [2014] found strong near-inertial currents generated by accelerating and decelerating wind stress in the unidirectional trade wind regime in the southeast Pacific. Arabian Sea during the southwest monsoon presents a similar scenario as *Weller et al.* [2014], since we observe strong near-inertial currents in the mixed layer generated by the variation in wind magnitude, while the direction mainly stays southwest.

The near-inertial currents are uniform in the mixed layer but decay in the transition layer. Since the mixed layer is shear free at near-inertial frequencies, the bandpassed momentum equations for a slab-like layer are used to derive a one-dimensional NIKE budget. The NIKE budget in the mixed layer constitutes of an energy source from the wind Π_W that forces the mixed layer, the rate of change of near-inertial KE in the mixed layer $\frac{d(NIKE_{ML})}{dt}$, a residual flux Π_R, estimated as a difference between the energy input and energy change in the mixed layer, and a term Π_H that accounts for the MLD variation.

During the strong wind events a significant amount of energy from the wind increases the amplitude of the near-inertial currents. Large energy input during these events increases the NIKE of the mixed layer, but we observe a decrease in NIKE after two inertial periods. This decrease in NIKE is due to the subsequent increase in energy losses in the mixed layer.

The NIKE budget discussed here is somewhat different than examined in PF06. In PF06 Π_W and Π_R balance each other and kinetic energy change in the mixed layer plays a minor role. In our case the kinetic energy change in the mixed layer is not always insignificant, though it decays in about two inertial periods. This difference may stem from the fact that the steady unidirectional forcing in the Arabian Sea is different than the resonant forcing events discussed in PF06.

The residual Π_R from the mixed layer budget is important to the evolution of NIKE of the transition layer. When dissipation and radiation losses are small in the mixed layer Π_R acts as a source of energy to the transition layer. We find such a case during event A (14–25 May) when wind-stress is weak and transition layer is thick. The NIKE change in the transition layer balances Π_R over the period 14–23 May. This suggests that the energy from the mixed layer can sometimes energize the transition layer as well, so that a loss term in the mixed layer becomes a source of energy to the transition layer. Since energy loss in the mixed layer is high during the other two events (B and C), Π_R is large but the change in NIKE in the transition layer is negligible.

For this data set, the mixed layer defined using a temperature criterion is also well mixed in momentum. We find that the bulk shear across the transition layer is dominated by near-inertial shear even though the wind is unidirectional during the monsoon. Since near-inertial currents in the mixed layer primarily arise due to change in wind stress magnitude with time, the alignment of wind stress and the transition layer shear explains the near-inertial spikes very well.

Appendix A: Comparison of Different Estimates of Π_W

In this section, we calculate different estimates of windwork Π_W by *D'Asaro* [1985](D85, hereafter), *Alford* [2003] (A03, hereafter), and PF06 and compare them with our estimate in (5). Although different estimates of Π_W have about the same mean, the instantaneous values are different (Figure 11). In the following we discuss this in detail.

Assuming a constant MLD, D85 derives Π_W using both hourly and 3 hourly wind stress as,

$$\Pi_{WD85} = -Re\left[\frac{Z_I}{(r+if)^*}\frac{d\tau^*}{dt}\right], \qquad (A1)$$

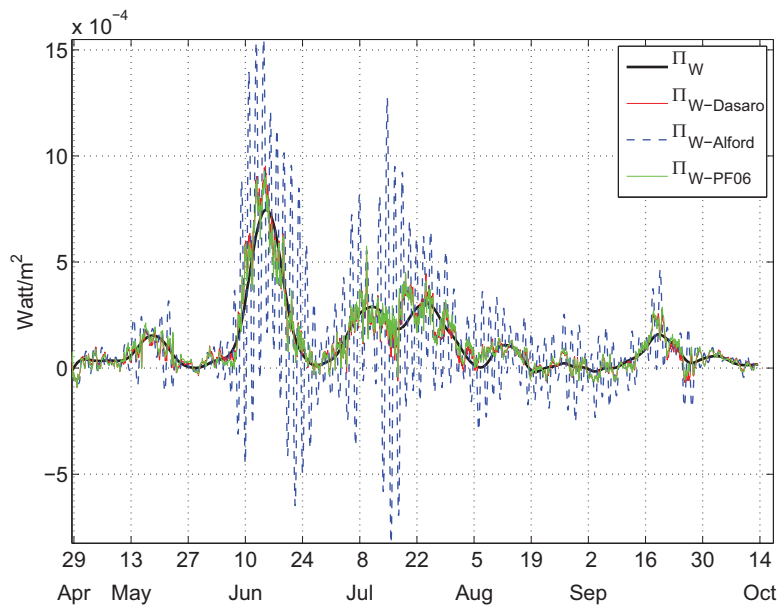where τ is the observed wind stress and r parameterizes damping in the mixed layer.

Figure 11. Different estimates of Π_W after applying a running average over four inertial periods. $\Pi_{WAlford}$ shows more variance compared to the other estimates.

A03 uses a simplified expression for the windwork as,

$$\Pi_{WA03} = Re[Z_I \tau^*]. \tag{A2}$$

Both D85 and A03 calculate Π_W using near-inertial current Z_I, estimated as a difference between the total current Z and the time-varying Ekman current $Z_E = T_W/(r+if)$ as, $Z_I = Z - Z_E$.

Near-inertial current estimated this way is noisy and incorporates high frequency components. Therefore, Z_I estimated by A03 and D85 does not match the bandpassed Z_I used in our estimate.

PF06 isolates Z_I from the total current using a band pass filter and estimates Π_W as,

$$\Pi_{WPF06} = -\rho_0 HRe\left[\frac{Z_I^*}{if}\frac{d}{dt}\left(\frac{T_W}{H}\right)\right]. \tag{A3}$$

Rather than using near-inertial components of wind stress as used in our expression, PF06 calculates (A3) using total wind stress and a 10 day smoothed MLD. All these estimates (A1–A3) reduce to (5) for inertially rotating wind ($\tau = \tau_0 e^{-ift}$), small damping (r small) and for a constant MLD.

We calculate equations (A1)–(A3)using mooring data. To estimate Π_W by D85 and A03 we use $r = 0.15f$. We average Π_W over four inertial periods and present it in Figure 11. This averaging restricts high frequency winds but allows low frequency components in wind to contaminate Π_{WA03}, Π_{WPF06} and Π_{WD85}. Among these three estimates Π_{WA03} is most noisy (Figure 11). The other two estimates (D85, PF06) use the time derivative of the total wind stress and have less variability than AO3 (shown in the following paragraph). High frequency components being cancelled out in the integration, cumulative windwork (P_W) is less noisy and is about the same for different estimates (Figure 12).

In this paragraph we analyze why estimates of Π_W are different. Since Π_{WPF06} and Π_{D85} are about the same (Figure 11) when MLD is constant and r is small, we only compare Π_{WD85}, Π_{WA03} and Π_W. For simplicity we consider the total wind stress τ as the sum of low frequency ($\tau_L e^{-i\omega_L t}$), high frequency ($\tau_H e^{-i\omega_H t}$) and inertial frequency components ($\tau_I e^{-ift}$),

$$\tau = \tau_H e^{-i\omega_H t} + \tau_L e^{-i\omega_L t} + \tau_I e^{-ift}, \tag{A4}$$

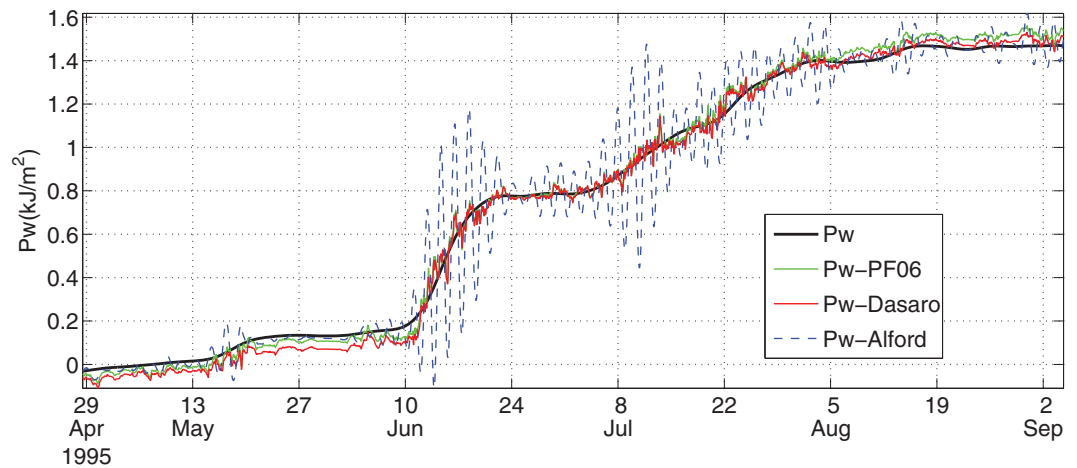where $\omega_H > f > \omega_L$. Combining (A1) and (A4) we obtain,

Figure 12. P_W (integrated Π_W) for PF06 (green), D85 (red) and A03's (blue) and our estimate (black).

$$\Pi_{WD85} = -Re\left[\frac{|Z_I|}{(r+if)^*}\left(i\omega_H\tau_He^{i(\omega_H-f)t}+i\omega_L\tau_Le^{i(\omega_L-f)t}+if\tau_I\right)\right], \qquad (A5)$$

where $Z_I=|Z_I|e^{-ift}$ is the inertial current. Averaging (A5) over four inertial periods filters out the high frequency variations and we obtain,

$$\Pi_{WD85} = -Re\left[\frac{|Z_I|}{(r+if)^*}\left(i\omega_L\tau_Le^{i(\omega_L-f)t}+if\tau_I\right)\right]. \qquad (A6)$$

This averaging acts as a low pass filter and allows only low frequency components. Assuming a constant mixed-layer depth H and small dissipation $r \ll f$ in the mixed layer, (A6) reduces to,

$$\Pi_{WD85} = -Re\left[\frac{|Z_I|}{-if}\left(i\omega_L\tau_Le^{i(\omega_L-f)t}+if\tau_I\right)\right], \qquad (A7)$$

or

$$\Pi_{WD85} = |Z_I|\tau_I+Re\left[|Z_I|\tau_L\left(\frac{\omega_L}{f}\right)e^{i(\omega_L-f)t}\right]. \qquad (A8)$$

Similarly following the above approach (A2) becomes,

$$\Pi_{WA03} = |Z_I|\tau_I+Re\left[|Z_I|\tau_Le^{i(\omega_L-f)t}\right], \qquad (A9)$$

and considering H to be almost constant (to simplify our calculation), (A3) becomes,

$$\Pi_{WPF06} = |Z_I|\tau_I+Re\left[|Z_I|\tau_L\left(\frac{\omega_L}{f}\right)e^{i(f-\omega_L)t}\right]. \qquad (A10)$$

Clearly, (A8), (A9) and (A10) differ by a factor $\frac{\omega_L}{f}$. The factor $\frac{\omega_L}{f}$ being less than unity, Π_{WA03} is larger than Π_{WD85} and Π_{PF06}. Since our estimate $\Pi_W=|Z_I|\tau_I$ does not have energy associated with low-frequency components of wind stress, it is different than the other estimates.

Appendix B: Scale Analysis of Interfacial Friction

Following *Burchard and Rippeth* [2009] and *Brannigan et al.* [2013], the interfacial drag term can be parameterized as, $c_ih^2S^2=\kappa S_{if}$, where κ and S_{if} are interfacial eddy viscosity and shear. With $S_{if}\approx S=10^{-4}\ s^{-1}$, $H=50$ m, $h_I=30$ m and a typical interior eddy viscosity $\kappa=10^{-5}\ m^2\ s^{-1}$, we obtain dimensionless interfacial drag coefficient of 10^{-4}. For wind stress $\tau_w=0.1$ N/m^2 and a typical $h=60$ m the shear production term $P(S^2)$ is $O(10^{-9})$ and the dissipation $D(S^2)$ is $O(10^{-16})$. Therefore $D(S^2)$ is not important to the shear evolution in the two-layer model.

References

Alford, M. H. (2003), Improved global maps and 54-yr history of wind work on ocean inertial motions, *Geophys. Res. Lett.*, *30*(8), 1424, *doi*: 10.1029/2002GL016614.

Alford, M. H., M. C. Cronin, and J. M. Klymak (2012), Annual cycle and depth penetration of wind-generated near-inertial internal waves at ocean station Papa in the Northeast Pacific, *J. Phys. Oceanogr.*, *42*, 889–909.

Brannigan, L., Y. D. Lenn, T. P. Rippeth, E. McDonagh, T. K. Chereskin and J. Sprintall (2013), Shear at the base of the oceanic mixed layer generated by wind shear alignment, *J. Phys. Oceanogr.*, *43*, 1798–1810.

Burchard, H., and T. Rippeth (2009), Generation of bulk shear spikes in shallow stratified tidal seas, *J. Phys. Oceanogr.*, *39*, 969–985.

D'Asaro, E. A. (1985), The energy flux from the wind to near-inertial motions in the surface mixed layer, *J. Phys. Oceanogr.*, *15*, 1043–1059.

Dohan, K., and R. E. Davis (2011), Mixing in the transition layer during two storm events, *J. Phys. Oceanogr.*, *41*, 42–66.

Fairall, C. W., E. F. Bradley, J. S. Godfrey, G. A. Wick, J. B. Edson, and G. S. Young (1996), Bulk parameterization of air-sea fluxes for tropical ocean-global atmosphere coupled-ocean atmosphere response experiment, *J. Geophys. Res.*, *101*, 3747–3764.

Fischer, A. S. (1997), Arabian Sea mixed layer deepening during the monsoon: Observation and dynamics, Master's thesis, MIT Press, Boston.

Fischer, A. S., R. A. Weller, R. L. Rudnick, C. C. Eriksen, C. M. Lee, K. H. Brink, C. F. Fox, and R. R. Leben (2002), Mesoscale eddies, coastal upwelling, and the upper-ocean heat budget in the Arabian Sea, *Deep Sea Res., Part II*, *49*, 2231–2264.

Gill, A. E. (1982), *Atmosphere-Ocean Dynamics, Int. Geophys. Ser.*, vol. 30, Academic, London, U. K.

Johnston, S., and D. L. Rudnick (2008), Observations of the transition layer, *J. Phys. Oceanogr.*, *39*(3), 780–797.

Plueddemann, A. J., and J. T. Farrar (2006), Observations and models of the energy flux from the wind to mixed-layer inertial currents, *Deep Sea Res., Part II*, *23*, 2351–2359.

Pollard, R. T., and R. C. Millard (1970), Comparison between observed and simulated wind-generated inertial oscillations, *Deep Sea Res. Oceanogr. Abstr.*, *17*, 813–821.

Price, J. F., R. A. Weller, and R. Pinkel (1986), Diurnal cycling: Observation and models of the upper ocean response to the diurnal heating, cooling, and wind mixing, *J. Geophys. Res.*, *91*, 8411–8427.

Silverthorne, K. E., and J. M. Toole (2008), Seasonal kinetic energy variability of near-inertial motions, *J. Phys. Oceanogr.*, *39*, 1035–1049.

Watanabe, M., and T. Hibiya (2002), Global estimates of the wind-induced energy flux to inertial motions in the surface mixed layer, *Geophys. Res. Lett.*, *29*(8), 1239, doi:10.1029/2001GL014422.

Weller, R., S. Majumder, and A. Tandon (2014), Diurnal restratification events in the Southeast Pacific trade wind regime, *J. Phys. Oceanogr.*, *44*, 2569–2587.